The Astrophysical Journal, 584:758–769, 2003 February 20

ON THE MAGNETIC FIELDS AND PARTICLE ACCELERATION IN CASSIOPEIA A

Jacco Vink[1]
Columbia Astrophysics Laboratory, Columbia University, MC 5247, 550 West 120th Street, New York, NY 10027;
jvink@astro.columbia.edu

and

J. Martin Laming
Naval Research Laboratory, Code 7674L, Washington, DC 20375; jlaming@ssd5.nrl.navy.mil
Received 2002 August 27; accepted 2002 October 30

ABSTRACT

We investigate the nonthermal X-ray emission from Cas A, using *BeppoSAX*, *Compton Gamma Ray Observatory* OSSE, and *Chandra* data. For the hard X-ray continuum we test the model proposed by Laming, which invokes nonthermal bremsstrahlung from electrons accelerated by lower hybrid plasma waves. The justification for this model comes from our determination of a lower limit to the average magnetic field of $B > 0.5$ mG. For such high magnetic fields, the synchrotron losses are severe enough that most of the electron populations responsible for the radio emission have maximum electron energies well below the limit for which X-ray synchrotron emission is important. However, we do suggest that the rim surrounding Cas A, seen in *Chandra* continuum images, is X-ray synchrotron emission. The width of this rim of 1.″5–4″ can be used to infer the magnetic field near the shock front, for which we estimate $B = 0.08$–0.16 mG and electron energies of ~57–40 TeV. This magnetic field strength is lower than the average magnetic field but higher than what may be expected from shocked interstellar medium, suggesting either a high magnetic field in the wind of the progenitor or rapid postshock field amplification by nonlinear growth of plasma waves. Combining the two magnetic field measurements, we have constructed a simple two-zone model. Most of the radio emission comes from inside Cas A, where the magnetic field is strong. In contrast, the inverse Compton emission is dominated by emission from near the shock front. Only for our lower limit on the magnetic field strength near the shock front is it possible to explain the recent detection of TeV emission by the High Energy Gamma Ray Astronomy experiment with inverse Compton emission, for which, in addition, we have to assume a rather high far-infrared photon density that should be twice as high as our best estimate of ~70 cm^{-3}. Pion decay is therefore likely to be the dominant emission from Cas A at TeV energies.

Subject headings: acceleration of particles — gamma rays: observations — ISM: individual (Cassiopeia A) — magnetic fields — shock waves — supernova remnants

1. INTRODUCTION

Supernova remnants have long been thought to be the source of cosmic rays with energies up to at least 10^{15} eV, at which there is a break in the observed cosmic-ray spectrum, usually referred to as the "knee." The recent discoveries of X-ray synchrotron and TeV emission from some supernova remnants support this long-held belief by confirming that electrons are accelerated to energies of at least a few TeV (Reynolds & Keohane 1999). This is still somewhat short of the "knee," but unlike for ions, the maximum electron energy may be limited by radiation losses.

SN 1006 has become the canonical example of a supernova remnant with X-ray emission dominated by synchrotron radiation from shock-accelerated electrons (Koyama et al. 1995). The presence of electrons in excess of 10 TeV is further supported by the detection of TeV emission with the CANGEROO Cerenkov detector (Tanimori et al. 1998). The observed TeV emission is most likely inverse Compton scattering by the same population of electrons that is responsible for the X-ray continuum (Tanimori et al. 1998), although there is some debate about this interpretation (Berezhko, Ksenofontov, & Völk 2002).

Another often mentioned candidate for an X-ray synchrotron emitting supernova remnant is Cas A. Its soft X-ray emission is not continuum dominated, but the observed emission above 20 keV cannot be explained by thermal bremsstrahlung and has therefore been attributed to synchrotron radiation (The et al. 1996; Allen et al. 1997; Favata et al. 1997). The detection of TeV emission by the High Energy Gamma Ray Astronomy experiment (HEGRA) is consistent with this interpretation, but pion decay associated with relativistic ions is an equally valid interpretation (Aharonian et al. 2001).

For Cas A the interpretation of both the hard X-ray and the TeV emission is critically dependent on the magnetic field strength. Equipartition arguments to explain the radio luminosity imply magnetic fields of $B \sim 0.4$–2 mG (Longair 1994; Wright et al. 1999), far in excess of the canonical value for the interstellar medium of 3 μG. The typical loss time of an electron with energy E due to synchrotron radiation is (e.g., Reynolds 1998)

$$\tau_{\rm loss} = \frac{635}{B^2 E}\ {\rm s}\ . \qquad (1)$$

For a magnetic field of 1 mG, a particle with $E = 8$ TeV loses its energy in 2 yr. For Cas A, 8 TeV is the maximum energy needed to explain the hard X-ray emission (Reynolds & Keohane 1999). The 2 yr lifetime is much shorter than the lifetime of Cas A, which is probably the remnant of a supernova that exploded in AD 1680 (Ashworth 1980).

[1] Chandra Fellow.

Similarly, a high magnetic field lowers the number density of relativistic electrons for a given radio brightness, which in turn implies a low inverse Compton contribution to the observed TeV emission.

One way out of this situation would be to assume that electrons are continuously being reaccelerated, but that seems unlikely. The radio morphology of Cas A shows a bright ring of radius $\sim 1\farcm8$, whereas the shock front, the primary site for cosmic-ray acceleration, is at a radius of $\sim 2\farcm6$. Moreover, detailed radio spectral index studies do not find evidence of reacceleration in bright radio knots, which are probably ejecta fragments penetrating the shell (Anderson & Rudnick 1996; Wright et al. 1999). These studies rather suggest that brightness variations are the result of variations in the magnetic field, which light up the diffuse relativistic electron population in various degrees.

Here we test an alternative interpretation of the hard X-ray emission with *BeppoSAX* Phoswich Detection System (PDS) data, namely, bremsstrahlung from electrons accelerated by lower hybrid waves (LHWs), which was suggested by Laming (2001a, 2001b). An additional argument for testing such a model is that *XMM-Newton* observations show that even above 10 keV, a substantial fraction of the continuum emission is not associated with the forward shock (Bleeker et al. 2001). The *BeppoSAX* data, in combination with *Compton Gamma Ray Observatory* (*CGRO*) OSSE data, also provide an upper limit on the bremsstrahlung from the electron cosmic-ray injection spectrum, from which a new lower limit on the average magnetic field strength can be obtained.

Nevertheless, we argue that X-ray synchrotron radiation does exist in Cas A and is coming from close to the forward shock, where it shows up as a narrow rim surrounding the remnant, observed in *Chandra* X-ray continuum images (Gotthelf et al. 2001). Interpreting the width of the rim as a typical length scale for synchrotron losses, we are able to constrain the magnetic field near the shock front. Our analysis supports the idea that the average magnetic field is close to its equipartition value, whereas we find that near the shock front the magnetic field is lower, but still an order of magnitude higher than what may be expected from shocked interstellar medium ($\sim 10^{-5}$ G). We discuss the implications of these values for the hard X-ray and TeV emission.

2. DATA AND OBSERVATIONS

Our analysis of the X-ray emission of Cas A is based on *BeppoSAX*/PDS data and archival *CGRO*/OSSE and *Chandra* data. The *BeppoSAX*/PDS (Frontera et al. 1997) and *CGRO*/OSSE (Johnson et al. 1993) instruments both consist of four phoswich detectors [NaI(Tl)/CsI(Na) scintillation detectors] behind two rocking collimators. They differ substantially, however, in energy range, field of view, and effective area. The *BeppoSAX*/PDS instruments cover an energy range of 15–300 keV, whereas the range is 50 keV to 10 MeV for *CGRO*/OSSE.

BeppoSAX observed Cas A for 500 ks in 2001 May and June in order to observe the 67.9 and 78.4 keV nuclear decay lines of ^{44}Sc, the nuclear decay product of ^{44}Ti. The detection of these lines at the 3–5 σ level, depending on the hard X-ray continuum model, was reported by Vink et al. (2001), which provides more details about the data set. Because of the rocking collimators, the effective exposure time is about half the observation time. Together with archival *BeppoSAX* data, the spectra used for our analysis here are based on a total effective PDS exposure of 311 ks.

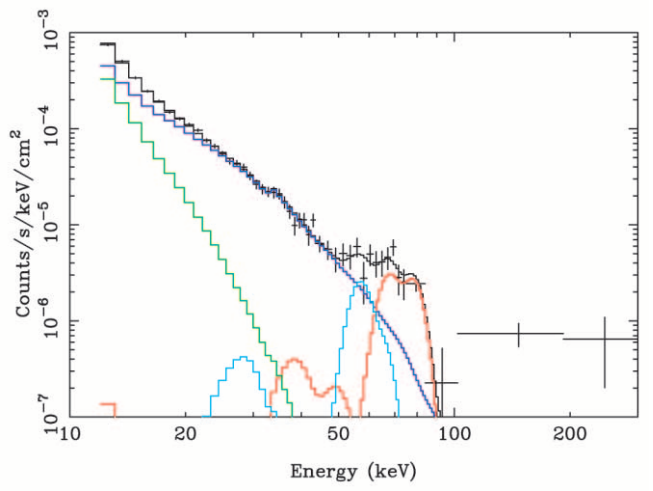

FIG. 1.—*BeppoSAX*/PDS spectrum of Cas A with the best-fit ^{44}Sc/nonthermal bremsstrahlung model. The individual emission components are ^{44}Sc line emission (*red line*), nonthermal continuum (*blue line*), thermal continuum (*green line*), and possible line contamination from collimator material (tantalum: *cyan line*). The observed count rate in each channel has been divided by the effective area in order to yield approximate flux densities.

The spectrum, as presented in Vink et al. (2001), clearly shows the hard X-ray spectrum with a bump associated with the ^{44}Sc line emission. Marginal (2 σ) residual emission around 60 keV is possibly caused by fluorescent tantalum K-shell emission, as a result of cosmic rays interacting with the collimator, which consists of tantalum with a thin copper-tin bilayer. Some residual emission above 100 keV is not easily explained (e.g., Figs. 1 and 2). It may be intrinsic to Cas A, but some instrumental contamination seems more likely. The residual emission peaks around 200 keV but is not narrow enough to be caused by fluorescent line emission from any particular material. There are no other similar deep *BeppoSAX* observations with a moderate hard X-ray brightness such as in Cas A that would allow us to identify possible instrumental features at this level.

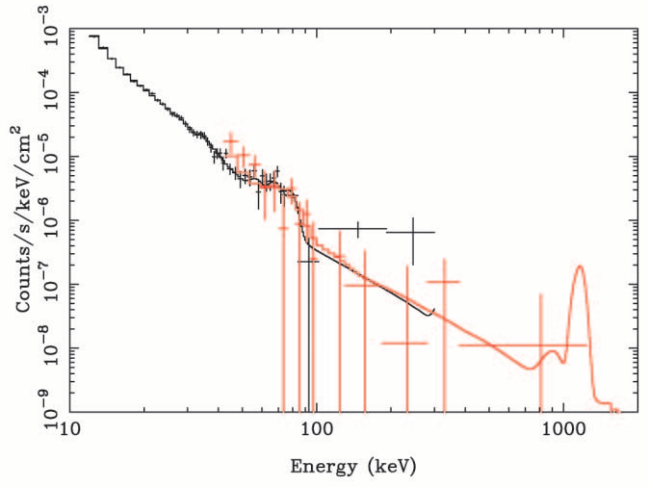

FIG. 2.—Best-fit model that combines the LHW/^{44}Sc with the electron cosmic-ray injection spectrum. Shown are the *BeppoSAX*/PDS (*black line*) and *CGRO*/OSSE (*red line*) spectra of Cas A.

Although the residual emission above 100 keV is statistically not very significant, one of our concerns is to obtain an upper limit on the emission above 100 keV in order to obtain a lower limit to the average magnetic field in Cas A. We therefore included archival *CGRO*/OSSE spectra in our analysis. Moreover, the effective area of the instruments peaks around 250 keV, making it useful for constraining the emission of Cas A above 100 keV. Cas A was observed several times by *CGRO*/OSSE (see The et al. 1996). We added all available Cas A spectra and averaged the corresponding response matrices. The observations were made during the viewing periods 34–815 with a total exposure of 909 ks.[2]

In addition to hard X-ray data, we used a deep (50 ks) archival *Chandra* observation with the ACIS-S3 chip to complement our analysis. The observation was made in 2000 January. The same data were used by Hwang, Holt, & Petre (2000). For our analysis we used level 2 archival data products, generating spectra and calibration products with the standard *Chandra* software package CIAO, Version 2.2.1.

3. THE LOWER HYBRID ELECTRON ACCELERATION MODEL

Cas A's morphology indicates a complicated, turbulent hydrodynamical structure. Radio, optical, and X-ray images all show many bright knots on top of more diffuse emission. As the forward or reverse shocks strike and illuminate these features, secondary shocks split off from these primary shocks and propagate back into the already shocked circumstellar or ejecta plasma. In this way, shocks may propagate across the likely region of high magnetic field at the contact discontinuity, where field amplification by Rayleigh-Taylor instability may occur. The acceleration of electrons by LHWs generated by these shocks has been considered by Laming (2001a, 2001b). Bremsstrahlung emitted by these accelerated electrons was shown to provide a very good match to the hard X-ray continuum of Cas A, using the ~50 ks of *BeppoSAX*/PDS data that were available at the time.

LHWs are electrostatic ion oscillations directed within an angular range $\pm\omega_{\rm pi}/\omega_{\rm pe}$ of the direction perpendicular to the magnetic field, where $\omega_{\rm pe}$ and $\omega_{\rm pi}$ are the electron and ion plasma frequencies, respectively. The electron screening that would usually damp such oscillations is inhibited by the magnetic field, giving a criterion on the electron temperature that the electron gyroradius be smaller than the wavelength divided by 2π. Since $\omega/k_\perp \ll \omega/k_{||}$, the wave can simultaneously be in resonance with ions moving across the magnetic field lines and electrons moving along them. Consequently, energy equilibration between ions and electrons may proceed at a much faster rate than by Coulomb collisions alone and saturate when the electron thermal pressure is equal to the magnetic pressure. Such processes have been considered in the context of two-temperature accretion flows by Begelman & Chiueh (1988). Here cross-field ion motions are produced by a combination of curvature and diamagnetic drift, and the magnetic field is presumably generated by a magnetorotational instability (Balbus & Hawley 1992, 1998; Quataert, Dorlan, & Hammet 2002), the critical issue being whether sufficient electron-ion equilibration can occur to destroy advection-dominated accretion flows or similar solutions for the accretion flow. In dilute plasmas where the electron acceleration time is much shorter than the electron-electron collision time, a non-Maxwellian electron distribution in the component of velocity along the magnetic field can result. This has been modeled numerically using particle-in-cell simulations by Shapiro et al. (1999) for application to cometary X-rays and analytically by Vaisberg et al. (1983) and Krasnosel'skikh et al. (1985). LHWs generated by a modified two-stream instability and the resulting accelerated electrons were all observed in comet Halley (Klimov et al. 1986; Gringauz et al. 1986). Bingham et al. (2000) considered LHWs in supernova remnants, and Laming (2001a, 2001b) applied the analytic formulations, which agree well with the numerical work, to the case of accelerated electrons in Cas A. The non-Maxwellian electron distribution function depends on two parameters, the overall normalization (i.e., the fraction of plasma electrons that are accelerated) and the maximum electron energy in the distribution. In our fitting we treat these both as free parameters. A demonstration of how these variables are related to other physics of the Cas A plasma, and hence can be determined, is given in the Appendix.

We fitted the predicted spectrum, calculated as in Laming (2001a) but with a relativistic bremsstrahlung cross section taken from Nozawa, Itoh, & Kohyama (1998), to the observed *BeppoSAX*/PDS X-ray spectrum. Apart from the nonthermal bremsstrahlung spectrum, several other components, which are likely to contribute to the hard X-ray emission, are included in the spectral model. At the low end of the hard X-ray spectrum, the tail of the thermal bremsstrahlung with $T_e = 4 \times 10^7$ K is expected to contribute to the spectrum. In addition, ^{44}Sc line emission at 68 and 78 keV is expected, as a result of the decay of ^{44}Ti synthesized during the explosion (Vink et al. 2001; Iyudin et al. 1994). The line fluxes of the two nuclear transitions are expected to be almost identical. A broadening corresponding with a velocity dispersion of 5000 km s^{-1} was included. A residual feature around 60 keV in the observed spectrum may be attributed to cosmic-ray–induced fluorescence from the tantalum collimator and was modeled by delta functions corresponding to Ta Kα (57 keV) and Kβ (65 keV) with a ratio of 4 : 1.[3] The spectrum and best-fit model are shown in Figure 1, and model parameters are given in Table 1.

The parameter values indicate that electrons are possibly accelerated up to ~95 keV. The model gives a very good fit to the spectrum up to 100 keV. However, it does not describe the emission observed above 100 keV. As discussed above, the data above 100 keV may be less reliable, and the low flux point around 100 keV suggests that the actual continuum emission is indeed curved, as predicted by the LHW model.

In Table 1 we also list for comparison the parameters for a simple power-law continuum spectrum and the X-ray synchrotron models available in the spectral fitting package XSPEC (Arnaud 1996): SRCUT and SRESC (Reynolds 1998; Reynolds & Keohane 1999). The SRCUT model is a very simplified model of X-ray synchrotron emission from a relativistic electron distribution with an exponential cutoff. In reality, the cutoff energy is likely to vary from place to

[2] In addition to the observations listed in The et al. (1996), this means VP 617, 715, 810, 814, and 815.

[3] See the X-ray data booklet (Thompson 2001).

TABLE 1
SUMMARY OF MODEL FITS TO THE *BeppoSAX*/PDS SPECTRUM

Parameter	LHW Model	SRCUT	SRESC	Power Law
Norm continuum[a]	0.058 ± 0.002	2522	2522	2.37 ± 0.2
Power-law index				-3.32 ± 0.05
$E_{\max}/E_{\rm cutoff}$ (keV)	95 ± 5	1.21 ± 0.01	3.42 ± 0.02	
Norm thermal emission[b]	0.62 ± 0.02	7.6 ± 3.3	0.0 (<2.5)	0.0 (<17)
^{44}Sc line flux (10^{-5} photons cm^{-2} s^{-1})	3.2 ± 0.3	2.7 ± 0.4	2.9 ± 0.4	2.1 ± 0.4
Ta Kα flux (10^{-5} photons cm^{-2} s^{-1})	2.4 ± 0.7	2.6 ± 0.8	2.8 ± 0.8	1.4 ± 0.0
χ^2/dof	273.1/251	273.0/252	289.3/252	267.5/251

[a] The normalization for the LHW model is defined as $10^{12} n_{\rm H} n_e V/4\pi d^2$ cm^{-5}. The normalization for the synchrotron models is fixed to the radio flux density at 1 GHz for the epoch 2000, and the radio spectral index is 0.775. These values are based on a compilation of radio data and include the effect of the secular flux decrease of Cas A (Baars et al. 1977). The normalization for the power-law model is photons s^{-1} keV^{-1} at 1 keV.

[b] The normalization is defined as $10^{12} n_{\rm H} n_e V/4\pi d^2$. The temperature was fixed to 4×10^7 K. Note that this definition assumes solar abundances, which is not applicable for Cas A, so care should be taken before using it to calculate electron densities.

place, giving a more gradual decrease in slope. Moreover, as explained in § 1, for the bulk of the relativistic electrons, at a remote distance from the shock front, the maximum electron energy is probably far below what is needed to produce X-ray synchrotron emission. The SRESC model takes these spatial effects into account, assuming a Sedov model for the evolution of the supernova remnant. Although SRESC is more physical, it may not be readily applicable to Cas A, which has large magnetic field gradients and is not well described by the standard Sedov model (Vink et al. 1998).

The LHW model is in a similar way somewhat oversimplified, since here it is also likely that maximum energies vary within the remnant, depending on local conditions such as the local shock velocity, obliquity, and ion composition. Nevertheless, given the limited number of parameters, the model fits very well. Note that the spectral slope between 20–50 keV is a property of the model and not a free parameter.

Finally, note that using the LHW model results in 50% higher ^{44}Sc line fluxes than using a power-law continuum, a result of the continuum curvature predicted by both models. The higher ^{44}Sc line flux is close to the latest *CGRO*/COMPTEL measurements of the ^{44}Ca line flux (Schönfelder et al. 2000) and translates into a synthesized ^{44}Ti mass of $1.8 \times 10^{-4}\ M_\odot$ for a distance of 3.4 kpc (Reed et al. 1995) and a ^{44}Ti decay time of 85.4 yr (Ahmad et al. 1998; Görres et al. 1998; Norman et al. 1998).

4. A NEW LOWER LIMIT TO THE AVERAGE MAGNETIC FIELD

The LHW model is attractive to consider for Cas A because of its high magnetic field strength, which is estimated to be ~1 mG, based on the assumption of equipartition of the relativistic particle population and the magnetic field energy (e.g., Longair 1994). Although there is no compelling physical reason why the equipartition assumption should be valid, estimates based on the absence of gamma-ray emission from Cas A support a value of the magnetic field in excess of what might be expected from a shock compression of the interstellar magnetic field (Cowsik & Sarkar 1980). The most recent estimate of the magnetic field is based on the upper limit obtained by *CGRO*/EGRET, suggesting $B > 3.5 \times 10^{-4}$ G (Esposito et al. 1996; Atoyan et al. 2000). This value is derived by comparing the radio synchrotron flux density with the expected bremsstrahlung from the relativistic electrons responsible for the radio emission.

Here we use essentially the same method, but less directly, since we use an extrapolation of the relativistic electron population to energies observed by *BeppoSAX*/PDS and *CGRO*/OSSE. The extrapolation used is similar to the one by Asvarov et al. (1990) and assumes that the electron *momentum* spectrum is a power-law distribution, as is expected for an electron population generated by first-order Fermi acceleration (Bell 1978). This means that the *energy* spectrum flattens at nonrelativistic energies. The electron cosmic-ray injection spectrum is not well known, but models indicate that at lower energies the spectrum is steeper than expected from extrapolating the relativistic spectrum (Bykov & Uvarov 1999). In that case, our upper limit on the cosmic-ray normalization is too high, which translates into too low a lower limit.

Of more concern is the role of energy losses on the shape of the spectrum, since it tends to flatten the low-energy end of the spectrum. We checked the signature of adiabatic losses on the spectrum and found that it does affect the spectrum mostly at mildly relativistic energies, where it results in a steeper spectrum at low energies, is flatter at intermediate energies, and then assumes the original power-law index at extreme relativistic energies. We did not take the steepening into account, since we do not know how much the average electron spectrum is affected by it. However, if there is a steepening, it makes our estimates too conservative. The other most dominant loss factor between 100 and 1000 keV in the ionized plasma of the remnant is electron-electron collisions. For an electron temperature of 4×10^7 K and density of 20 cm^{-3}, the loss time of a 100 keV electron is ~200 yr, rapidly increasing to ~500 yr for 200 keV (Huba 1994). These loss times are comparable to or larger than the average plasma age of Cas A, indicating that nonadiabatic losses are likely to be small.

The synchrotron flux density for a relativistic electron power-law distribution, with energy index q, is given by (Blumenthal & Gould 1970)

$$F_\nu = 1.70 \times 10^{-21} a(q) \frac{\kappa V}{4\pi d^2} \times B^{(q+1)/2} \left(\frac{6.26 \times 10^{18}}{\nu} \right)^{(q-1)/2}, \quad (2)$$

where κ is the particle normalization, V the emitting volume, d the distance, B the magnetic field, and $a(q)$ a factor tabulated in Blumenthal & Gould (1970).

Bremsstrahlung from the same population of electrons, which flattens at nonrelativistic energies, scales with the factor $\Sigma_i n_i Z_i^2 \kappa V/4\pi d^2$, where $\Sigma_i n_i Z_i^2$ indicates the sum of densities of all the ion species with charge Z_i. Therefore, from the combination of synchrotron emission and bremsstrahlung and an estimate of $\Sigma_i n_i Z_i^2$, we can estimate κ and B.

The radio spectrum of Cas A has a spectral index of $\alpha = -0.78$, and based on a compilation of radio data (e.g., Baars et al. 1977), we estimate a radio flux density of 2522 Jy at 1 GHz for the epoch 2000. The spectral index indicates an electron energy spectrum with $q = 2.56$ at relativistic energies and flattening to 1.77 at nonrelativistic energies, resulting in an X-ray photon index of -2.2. This is at odds with the observed spectral index of -3.3, which means that 100 keV must have a different origin, taken here to be bremsstrahlung from LHW-accelerated electrons. We adopt the LHW model and try to obtain an upper limit on the emission from an additional component with a power-law slope of -2.2 from the combined *BeppoSAX* and *CGRO*/OSSE data (Fig. 2).

The best-fit normalization for such a power-law spectrum is $(4.0 \pm 1.5) \times 10^{-7}$ photons s^{-1} keV^{-1} cm^{-2} at 100 keV, with a 2 σ upper limit of 6.2×10^{-7} photons s^{-1} keV^{-1} cm^{-2}. We measured the electron spectrum normalization more directly by fitting a model of bremsstrahlung from a relativistically correct power-law momentum spectrum, using the gaunt factors proposed by Haug (1997). The upper limit on the bremsstrahlung normalization obtained in this way is $\kappa \Sigma_i n_i Z_i^2 V/4\pi d^2 < 65$. Soft X-ray observations imply $\Sigma_i n_i Z_i^2 \simeq 20$ (Vink, Kaastra, & Bleeker 1996; Willingale et al. 2002a), which, combined with the bremsstrahlung normalization, gives for the average magnetic field $B > 0.5$ mG.[4] This is higher than the value derived by Atoyan et al. (2000) from the *CGRO*/EGRET upper limit, especially taking into account that they assumed a higher value for $\Sigma_i n_i Z_i^2$. Note that the above lower limit is not a volume average but is based on the ratio $\langle \kappa B^{(q+1)/2} \rangle / \langle \kappa \Sigma_i n_i Z_i^2 \rangle$. The derived lower limit is in good agreement with equipartition of magnetic and cosmic-ray energy.

5. THE MAGNETIC FIELD NEAR THE SHOCK FRONT

The high average magnetic field in Cas A is inconsistent with simple shock compression of the interstellar magnetic field and indicates that the magnetic field inside the remnant must have been enhanced by turbulence. A likely place for turbulence is the contact discontinuity, which may explain why the radio emission has a bright ring of emission, since this is the region in the remnant where magnetic field amplification is important. A similar argument was used by Anderson & Rudnick (1996) to explain why radio knots have the same radio spectral index as the surrounding diffuse emission; the enhanced magnetic field lights up the background electron population. One may wonder, then, what the initial interstellar magnetic field was before turbulent magnetic field amplification.

[4] This replaces the value reported in Vink & Laming (2003), in which we missed a factor of 4π in the synchrotron normalization, eq. (2) (e.g., Ginzburg & Syrovatskii 1965).

An estimate can be derived from the observation of the shock front of Cas A by *Chandra*. In the X-ray continuum band from roughly 4.5 to 6 keV, Cas A seems bound by a narrow rim of emission, which marks the onset of radio emission. The narrowness of the rim indicates strong limb brightening of a layer, which must have some special emission properties. The fact that the radio and X-ray morphology are dissimilar as far as this rim is concerned seems to argue against a synchrotron origin for the X-ray emission; see, e.g., Gotthelf et al. (2001). However, this is not true if the width of the rim is a result of the limited lifetime of the ultrarelativistic electrons as soon as they are swept away from the shock front. Farther inside the shock, the maximum energy of the electrons has so much decreased that no X-ray synchrotron emission is produced anymore. This is not the case for the radio emission, caused by electrons with much lower energies, for which synchrotron and inverse Compton losses are negligible (e.g., Wright et al. 1999). This behavior can be seen in the models by Reynolds (1998), in which the synchrotron-emitting shell is thinner at higher frequencies. The steady increase in radio emission toward the bright ring of emission may be the effect of the accumulation of relativistic electrons swept away from the shock front and a strong gradient of the magnetic field.

In this interpretation, most of the electron populations, which reside outside the X-ray rims, have a maximum energy cutoff well below 1 TeV, unless reacceleration is important. However, radio spectral-index measurements do not indicate any reacceleration of electrons by ejecta knots, which would likely lead to different indexes of radio knots and diffuse emission (Anderson & Rudnick 1996). Note that this also argues against the use for Cas A of the simple maximum curved synchrotron model employed by Reynolds & Keohane (1999), which merely assumes that all electron populations have the same energy cutoff and that the magnetic field is constant.

The rim is much narrower than the $\sim 1/12$ shock radius expected for plasma shocked with a factor of 4 compression ratio. That it is indeed consistent with X-ray synchrotron emission can be exemplified by a comparison of the X-ray continuum flux and radio flux of part of the rim in the northeast (see Fig. 3, Table 2). We used archival *Chandra* data to obtain a spectrum from this filament and determined that the X-ray continuum flux between 4 and 6 keV is 1.0×10^{-12} ergs s^{-1} cm^{-2} (2.1×10^{-7} Jy at 1.2×10^{18} Hz). We normalized an archival Very Large Array (VLA) radio map (epoch 1987) to a flux of 2522 Jy and extracted a flux density from the same region. Since the shock front may have moved between 1987 and 2001 by as much as 5″, we also extracted a flux from the same region but moved 5″ toward the center of the remnant. This yielded a flux density estimate between 3 and 6 Jy at 1 GHz, corresponding to a broadband spectral index of $\alpha = -1.15$ (the factor of 2 uncertainty in flux density is irrelevant over a frequency range of 9 decades). This is steeper than the radio spectral index of 0.78 and thus indicates that the X-ray flux density is below the extrapolation of the radio spectrum, consistent with the interpretation that part of the X-ray emission is synchrotron emission.

Indeed, not all X-ray emission is synchrotron, since the narrow rim displays line emission from Mg, Si, and S, which should be accompanied by bremsstrahlung as well. The line emission from the rim is, however, weaker and the spectrum harder than for the spectrum of a region just inside the rim

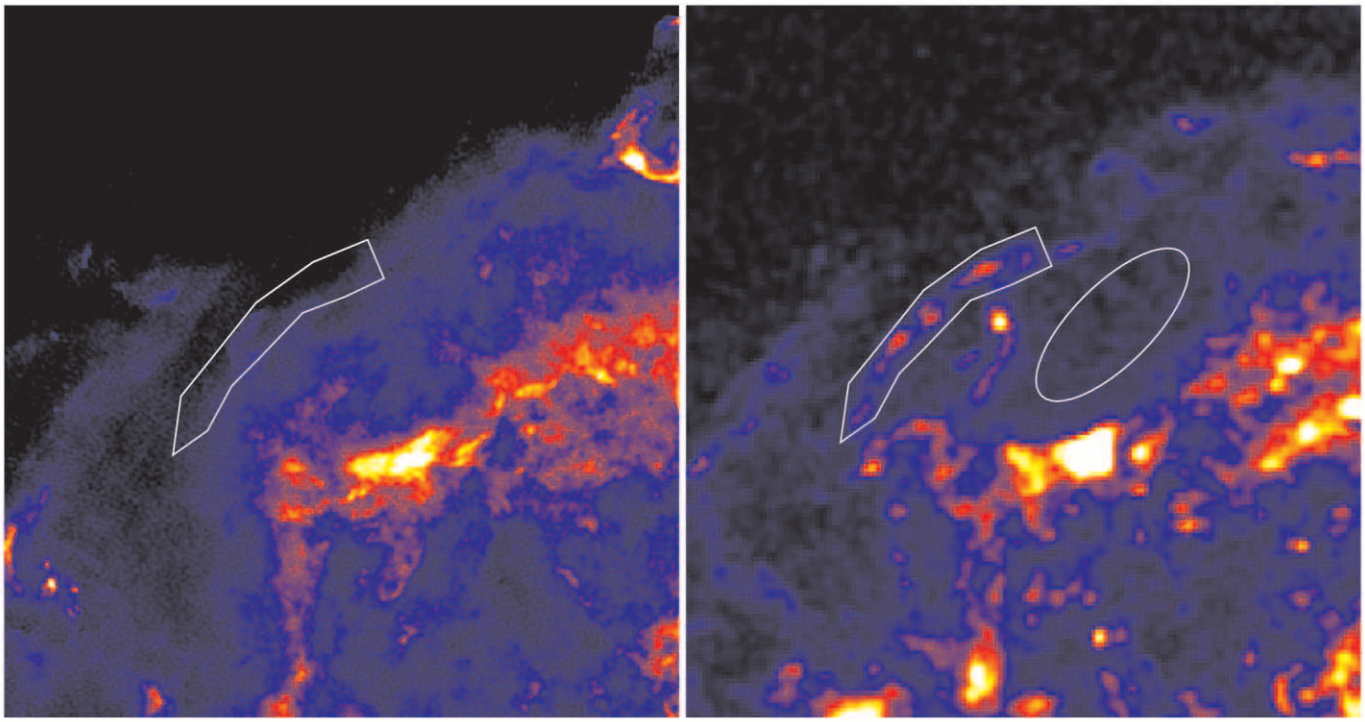

FIG. 3.—Detail of a VLA radio image (*left*) and *Chandra* ACIS X-ray image (*right*) from a compilation of continuum-dominated bands between 2.7 and 9 keV. The spectral extraction regions are indicated in the *Chandra* image (northeast rim and northeast inside rim).

(Table 2, Fig. 4). For example, fitting a thermal nonequilibrium model with an additional power law gives a spectral index of −2.2, whereas away from the rim, the spectral index is unconstrained but steeper than −4. Moreover, it is difficult to find another interpretation for the rim than synchrotron emission, since only energy losses can explain the narrow features. For a hot plasma, the losses are small, and the gradual ionization and possible equilibration of

TABLE 2

BEST-FIT PARAMETERS FOR SPECTRA FROM THE NORTHEAST RIM

Parameter	NE Rim	Both	Inside NE Rim
kT (keV)	3.7 ± 0.7		3.0 ± 0.4
$n_e t$ (10^{10} cm^{-3} s^{-1})	3.3 ± 0.5[a]		5.2 ± 0.6
Ne		$0.4^{+1.0}_{-0.4}$	
Mg		0.9 ± 0.4	
Si		4.5 ± 0.6	
S		4.3 ± 0.7	
Ar		4.4 ± 1.5	
Ca		5.4 ± 2.5	
Fe		2.2 ± 0.4	
Emission measure (10^{10} cm^{-5})[b]	3.0 ± 0.4		7.5 ± 1.0
Power-law index	-2.24 ± 0.05		-4.5 (<-4.3)[c]
Power-law norm (10^{-3} s^{-1}cm^{-2})[d]	2.5 ± 0.2		3.4 ± 0.6
Power-law contribution, 4–6 keV	84%		11%
$N_{\rm H}$ (10^{22} cm^{-2})		1.08 ± 0.03	
χ^2/ν	261/161		363/153

NOTES.—The spectral model consisted of the SPEX nonequilibrium ionization model (Version 1.10; see Kaastra et al. 1996) and a power-law continuum, in order to approximate the synchrotron radiation. The column density and abundances were first determined for the spectrum inside the northeast rim and subsequently applied to the rim spectrum. Following Vink et al. 1996, we set He and N abundances to 10 times solar (Anders & Grevesse 1989). The poorly constrained O abundance was coupled to Si; Ni was coupled to Fe. Errors correspond to 95% confidence intervals.

[a] Note that this value is roughly consistent with the synchrotron loss times, if the electron density is $n_e \sim 30$ cm^{-3}.

[b] The emission measure is defined as $n_{\rm H} n_e V/4\pi d^2$.

[c] The power-law slope was poorly constrained, but tended to be steep; we therefore fixed it to a value of 4.5. The lower limit corresponds to $\Delta\chi^2 = 4$.

[d] At 1 keV.

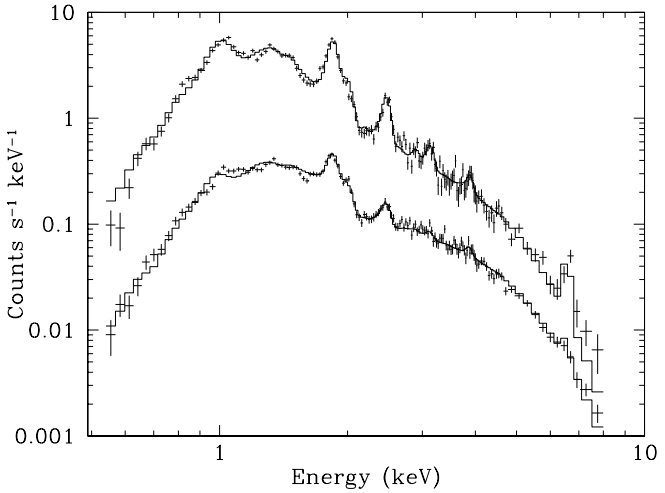

FIG. 4.—*Chandra* ACIS-S3 X-ray spectra of the narrow rim of emission (*bottom spectrum*) and from emission just inside the rim (×10; *top spectrum*). Note the lower equivalent width of the line emission from the spectrum of the rim (e.g., Table 2).

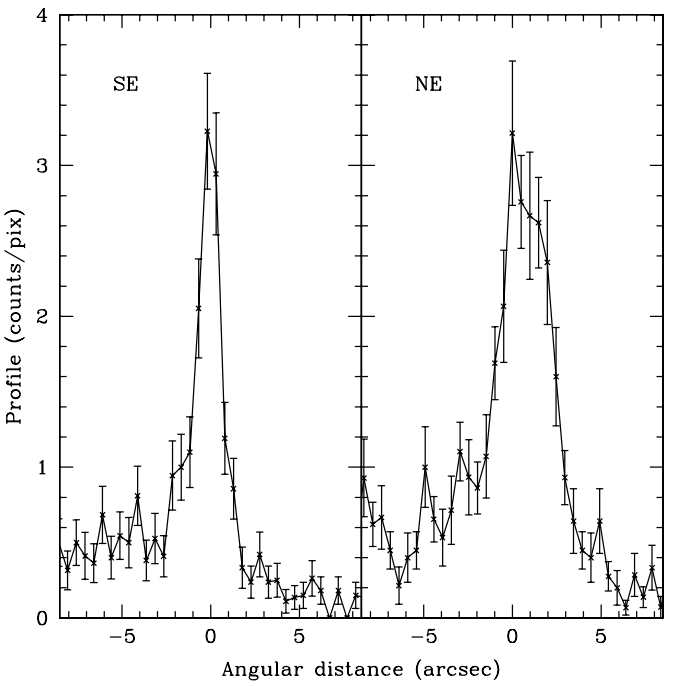

FIG. 5.—Emission profiles of the rim in the southeast (*left*) and northeast (*right*). The profiles were extracted using strips of 20 pixels wide (9″.8) from a *Chandra* image, which was a combination of continuum-dominated bands between 2.7 and 9 keV.

electrons and ions behind the shock would lead to a steady increase in intensity behind the shock, not in a sudden onset of emission followed by a rapid decline.

Interestingly, identifying the rims with X-ray synchrotron emission from recently accelerated electrons makes this aspect of Cas A very similar to SN 1006, where the X-ray synchrotron emission is coming from a similarly narrow rim of emission, as shown by archival *Chandra* data. For SN 1006, however, the continuum emission from the rims are dominating the total continuum emission, whereas for Cas A the X-ray continuum morphology shows that a substantial fraction of the X-ray continuum is associated with the bright ejecta shell. In SN 1006 the synchrotron emission comes mainly from the northeastern and southwestern limbs, which is usually interpreted as being caused by the large-scale orientation of the magnetic field (Reynolds 1998). For Cas A, however, we do not see such axisymmetry. This implies a much more randomly oriented magnetic field in the surrounding medium.

Assuming that the limb-brightened rim indeed emits X-ray synchrotron radiation, we can derive from the typical width of the rim the magnetic field behind the shock front and the typical electron energy responsible for the synchrotron radiation. The electron energy may be associated with the typical exponential cutoff energy of the electron spectrum, but the very nature of the losses makes it likely that a range of cutoff values exist. In an equilibrium situation, synchrotron and inverse Compton losses will steepen the spectrum by $\Delta q = -1$ (Longair 1994), but as soon as the electrons are sufficiently far removed from the shock front, the spectrum is more likely to have an exponential cutoff. An exponential cutoff is also more likely if the spectrum near the shock front is age limited instead of loss limited (Reynolds 1998).

The rims have a typical width of 1″.5–4″ and clearly stand out above the background and diffuse emission (Fig. 5). We can estimate a typical loss time from the widths by combining them with the plasma velocity away from the shock front. The shock velocity in Cas A has been estimated from proper motion studies using *Einstein* and *ROSAT* HRI X-ray images and is thought to be $v_s = 5200$ km s^{-1} (Vink et al. 1998). The velocity of plasma away from the shock front, for a standard shock compression ratio of 4, is $0.25v_s = 1300$ km s^{-1}. This value is consistent with X-ray Doppler shifts, which imply a velocity relative to the shock front of $\Delta v \sim 1400$ km s^{-1} (Willingale et al. 2002b). For a distance of 3.4 kpc, the measured widths of the rims correspond to a typical loss time of 18–50 yr.

The energy history of an electron with initial energy E_0, suffering synchrotron losses, is

$$E(t) = \frac{E_0}{1 + E_0 B^2 t/635} \ . \tag{3}$$

After a time τ (eq. [1]), the electron will have an energy $\frac{1}{2}E_0$, whereas higher energy electrons after the same amount of time will have energies $E'(\tau) \leq E_0$. The relation between the peak emitting frequency and electron energy is given by (Ginzburg & Syrovatskii 1965)

$$\nu_{\rm peak} = 1.8 \times 10^{18} B_\perp E^2 \ . \tag{4}$$

In reality, we have to take into account a range of frequencies, since the synchrotron emission function is broad.

The rim is best visible in the X-ray continuum dominated band of 4–6 keV and in some narrow bands in between line emission features. Taking 5 keV (1.2×10^{18} Hz) as the typical photon energy, we can combine equation (4) with equation (1) to obtain a typical electron energy of $E = 65$–91 ergs and $B = 0.16$–0.08 mG. The power-law slope of the *Chandra* spectrum near the shock is -2.2, which indicates that the photons are emitted by electrons close to the break in the electron distribution. In fact, using the SRCUT model (see also § 3), we derive for $B = 0.1$ mG, $E_{\rm break} \sim 25$ ergs. However, the spectrum is likely to be an integration of spectra with different break energies. Therefore, close to the shock front, $E_{\rm break}$ is likely to be higher.

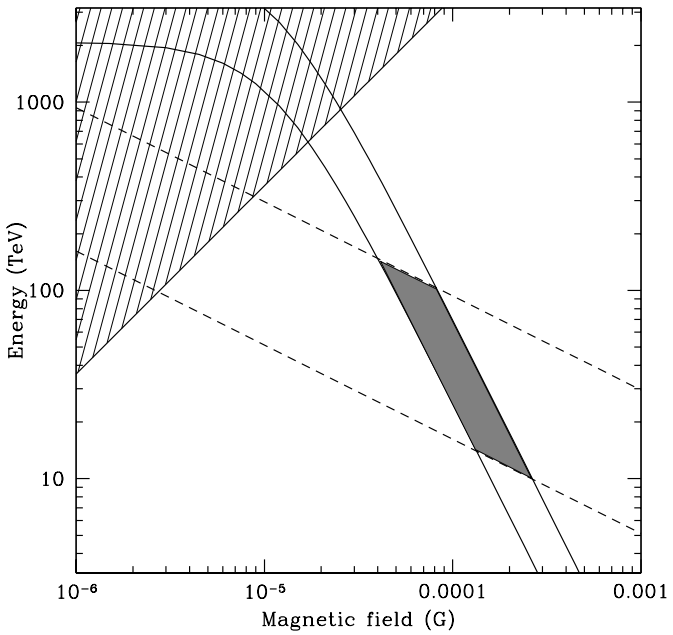

FIG. 6.—Most likely values of E_{max} and B just behind the shock front (*shaded region*). This area is formed by the two dashed lines, which mark the electron energies that contribute to the continuum emission around 5 keV, allowing for emission at 1/3 and 10 times the peak frequency for synchrotron emission, and the solid lines, which are formed by assuming that the width of the rims is determined by radiative losses (decay times of 18–50 yr and a shock velocity of 5200 km s^{-1} are assumed). The width of the rims should be at least larger than twice the gyroradius. This means that for a typical width of 3″, the hatched region is excluded.

In Figure 6 we have illustrated our estimates of magnetic field strength and electron energy graphically. Apart from synchrotron losses, we have also included inverse Compton losses. For this we have estimated the photon energy density from the cosmic microwave background and the far-infrared emission from Cas A itself, the latter being the most dominant factor. From the *IRAS* infrared fluxes listed by Braun (1987), we estimate a photon energy density of $u = 4.7 \times 10^{-12}$ ergs cm^{-3}, corresponding to an equivalent magnetic field of $B = 1.1 \times 10^{-5}$ G.

The estimates of the magnetic field near the shock front give values of roughly one-fifth of the average magnetic field strength and indicate a preshock magnetic field of $\sim(2\text{–}4) \times 10^{-5}$, a factor of 10 higher than the canonical interstellar medium value. This may hint at either a higher magnetic field surrounding Cas A, for instance because the wind of the Wolf-Rayet progenitor carried a high magnetic field, or that the presence of accelerated particles near the shock front has given rise to magnetic field amplification due to nonlinear plasma wave growth. The first hypothesis was suggested by Biermann & Cassinelli (1993) in order to explain the acceleration of cosmic rays by supernova remnants up to 10^{16} eV, for which high magnetic fields are necessary. The second hypothesis was suggested by Lucek & Bell (2000) for identical reasons.

6. THE MAGNETIC FIELD STRENGTH AND THE NATURE OF THE TeV EMISSION

The measured magnetic field strengths have important consequences for the gamma-ray emission from Cas A. For instance, our lower limit on the average magnetic field strength implies that the gamma-ray emission from bremsstrahlung is almost an order of magnitude below the *CGRO*/EGRET upper limit.

It is also understood that for the high magnetic field in Cas A, it is unlikely that the detected TeV emission is inverse Compton emission (Aharonian et al. 2001; Atoyan et al. 2000). We have investigated this important issue by constructing a two-zone model. Zone 1 is responsible for the bulk of the radio emission, such as the bright radio ring. It should have $B > 0.5$ mG according to the lower limit on the magnetic field. Since the electron population in this zone is old, no X-ray synchrotron emission is produced. We adopt a somewhat arbitrary maximum electron energy of 0.1 TeV, but in reality a range of values exists inside the remnant. The inverse Compton emission from this zone is negligible.

Zone 2 is responsible for the X-ray synchrotron emission from the rim and has $B \sim 0.08$–0.16 mG and $E_{max} \sim 40$–60 TeV. Based on our flux measurements, and assuming spherical symmetry, we estimate that the X-ray synchrotron emission should be less than one-third of the X-ray emission around 5 keV, but since we focused on a particularly bright part of the rim, 1/10 to 1/20 seem more likely values. Moreover, for $B = 0.08$ mG and an X-ray synchrotron flux contribution of one-third, the nonthermal bremsstrahlung flux at 100 keV is above the measured upper limit. This criterion is relaxed for higher magnetic fields near the shock front.

This two-zone model is different from the two-zone model proposed by Atoyan et al. (2000), for which the two zones relate to the radio knots and diffuse radio emission. We adopt here the view of Anderson & Rudnick (1996) that there are no intrinsic differences between the electron cosmic-ray populations of the radio knots and the diffuse emission, except that in the radio knots the magnetic field is stronger. Note that the electron cosmic-ray density is higher in zone 2. Zone 1 is brighter at radio wavelength because of the stronger magnetic field.

In order to estimate the inverse Compton emission, we need to estimate the photon density caused by Cas A's far-infrared emission. *IRAS* flux measurements (Braun 1987) indicate a total photon flux of $F_{ph} = 3.9 \times 10^5$ photons s^{-1} cm^{-2}, centered around 10^{13} Hz. The far-infrared emission is associated with ejecta (Lagage et al. 1996). Approximating the geometry by a sphere with radius similar to the ejecta, $r = 1.8$ pc, and assuming that half the number of photons spend an average time of r/c inside the sphere, we obtain for the photon density[5]

$$n_{ph} = \frac{3}{2}\frac{d^2}{r^2}\frac{F_{ph}}{c} = 72 \text{ cm}^{-3} , \quad (5)$$

where $d = 3.4$ kpc is the distance to Cas A. A similar reasoning gives a somewhat lower photon density for zone 2, but the photon field is much more anisotropic, on average coming from the direction of the remnant's center. For the spherical symmetry assumed, the anisotropy has no influence on the total inverse Compton emission, but since the maximum upscattering occurs for head-on collisions, most energetic inverse Compton emission from zone 2 will be directed toward the center of the remnant, giving rise to a centrally brightened morphology, despite the fact that according to our model, the dominant inverse Compton

[5] The other half of the photons escape directly, but all photons have to pass through zone 2.

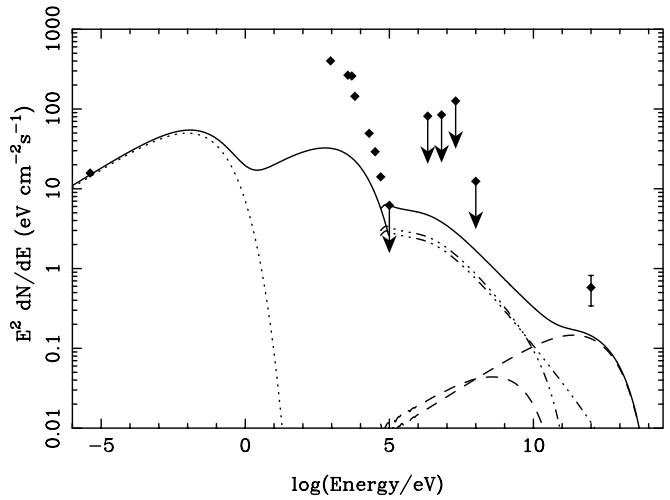

FIG. 7.—Simplified two-zone model of the broadband radiation from the cosmic-ray electron population, i.e., synchrotron radiation (*dotted line*), bremsstrahlung (*dot-dashed line*), and inverse Compton emission (*dashed line*). The solid line gives the total emission from both zones. The parameters near the shock front (zone 2) were chosen to be $B = 1.0 \times 10^{-4}$ G and $E_{\max} = 55$ TeV. For zone 1, $B = 0.5$ mG. The data points give the flux at 1 GHz, the X-ray continuum emission (*ASCA* and *BeppoSAX*), *CGRO*/COMPTEL (Strong et al. 2000), the *CGRO*/EGRET upper limit (Esposito et al. 1996), and the HEGRA detection (Aharonian et al. 2001).

emission is coming from a narrow shell near the shock front. In contrast, bremsstrahlung from the same electron population will show a ringlike morphology. Unfortunately, these interesting differences in morphology occur on the scale of arcminutes, which is currently beyond the reach of gamma-ray instruments.

Our two-zone model is illustrated in Figure 7, employing typical values for B and $E_{\rm break}$ near the shock front. The inverse Compton emission is completely dominated by the electrons in zone 2. In Figure 7 inverse Compton emission is well below the TeV flux seen by HEGRA. It is therefore likely that the TeV emission is dominated by pion decay. However, we cannot yet make a definitive statement regarding the inverse Compton emission. For lower values of the magnetic field, zone 2 is also the dominant source of bremsstrahlung by relativistic electrons. If the magnetic field is at the low end of our inferred magnetic field, $B = 0.08$ mG, and the far-infrared photon density is larger than 150 cm^{-3}, the HEGRA detection and the *BeppoSAX*–*CGRO*/OSSE upper limit on the nonthermal bremsstrahlung are still consistent with inverse Compton emission. The basic uncertainty in the photon density stems from the uncertain geometry, which for zone 2 may also include anisotropic photon emission. The combination of a low magnetic field and a rather high infrared photon density seems unlikely but is not impossible. Even lower magnetic fields in zone 2 are unlikely, since the nonthermal bremsstrahlung would exceed the upper limit reported in § 3.

7. CONCLUSION

We have provided estimates of the average magnetic field and the magnetic field near the shock front. The lower limit to the average magnetic field is based on the assumption that the electron spectrum follows a power-law distribution in momentum or is steeper than that at energies between 100 and 1000 keV.

The magnetic field strength near the shock front was measured from the width of the narrow rim surrounding Cas A in X-ray continuum images, assuming that the emission mechanism is synchrotron emission, and the width was determined by synchrotron losses. The contribution of the X-ray synchrotron emission to the X-ray continuum flux is less than one-third. This is supported by the X-ray morphology, which shows that even around 10 keV, a substantial part of the continuum is associated with the bright ejecta shell (Bleeker et al. 2001).

This justifies taking into consideration alternative models to synchrotron radiation for the hard X-ray emission of Cas A. This was done in § 2, in which we tested the lower hybrid wave model. The bremsstrahlung spectrum predicted for electrons accelerated by LHWs has a similar spectral slope, as is observed. The maximum energy to which the electrons are accelerated by this mechanism is ~95 keV, according to fits to the *BeppoSAX* data.

The estimated lower limit on the average magnetic field is 0.5 mG, whereas we find ~0.1 mG near the shock front. Therefore, even near the shock front the magnetic field strength is an order of magnitude above what is expected from shock compression of the canonical interstellar magnetic field of 3 μG. This can be explained by either a higher magnetic field strength in the medium surrounding Cas A, possibly as the result of the stellar wind of the progenitor (Biermann & Cassinelli 1993), or the magnetic field being rapidly enhanced near the shock front (Lucek & Bell 2000).

Electron energies close to the shock front may reach ~50 TeV or higher, but in contrast to Reynolds & Keohane (1999), we suggest that most of the cosmic-ray electrons responsible for the bright radio ring are in an environment with a high magnetic field, where because of synchrotron losses the cutoff energy is well below the energy at which X-ray synchrotron emission can be expected.

The high average magnetic field makes it likely that TeV emission from Cas A is dominated by pion decay (Atoyan et al. 2000), but there is some uncertainty, since in our two-zone model of Cas A it is still possible to obtain a high inverse Compton flux by assuming that the magnetic field is at the low end of what we have inferred from the X-ray rims, $B = 0.08$ mG, and using a higher far-infrared photon density of 150 cm^{-3}.

Future missions will improve on those results. For instance, the *Gamma-Ray Large Area Space Telescope* will probably be able to detect bremsstrahlung in the GeV range, which will provide a much more direct way of estimating the average magnetic field of Cas A.

As for the hard X-ray emission, the *International Gamma-Ray Astrophysical Laboratory* will not greatly improve the current measurement of the hard X-ray continuum emission, but by accurately measuring the ^{44}Ti-related line emission, it will constrain that component of the emission around 80 keV and thus indirectly improve our understanding of the continuum emission around 100 keV.

One of the consequences of our analysis is that the gamma-ray emission will be mostly associated with the outer rim of Cas A, not with the bright X-ray and radio shell. Unfortunately, the spatial resolution required to measure this will not be available in the near future.

Finally, as an interesting by-product of our analysis, we mention that the new modeling of the hard X-ray emission with the lower hybrid model yields revised values of the ^{44}Sc line emission at 68 and 78 keV, which correspond to a 50%

higher mass of ^{44}Ti synthesized in the explosion compared to what was reported by Vink et al. (2001), i.e., $M(^{44}\mathrm{Ti}) = 1.8 \times 10^{-4}\ M_{\odot}$. This is closer to the latest *CGRO*/COMPTEL measurements (Schönfelder et al. 2000).

J. V. was supported for this work by NASA through Chandra Postdoctoral Fellowship PF0-10011 issued by the *Chandra* X-ray Observatory Center (CXO), which is operated by the Smithsonian Astrophysical Observatory (SAO) for and on behalf of NASA under contract NAS8-39073. J. M. L. was supported by basic research funds of the Office of Naval Research. We acknowledge the use of the HEASARC (Goddard Space Flight Center), CXO (SAO), and NCSA Astronomy Digital Image Library archival facilities.

APPENDIX

In this appendix we want to demonstrate how free parameters in the fit of the model continuum (the maximum accelerated electron energy and the fraction of ambient electrons that are accelerated) are in principle determined by the plasma physics parameters of Cas A. The maximum electron energy is related to the maximum electric field that an LHW can develop and the time that an electron can spend in this field, governed by the thickness of the shock precursor. The fraction of electrons that may be accelerated is expected to be determined by a marginal stability criterion, i.e., the electrons will be accelerated until the heating of the ambient plasma produced by Coulomb collisions of the accelerated electrons violates the conditions necessary for LHWs to exist, i.e., until the electron gyroradius is less than the wavelength divided by 2π.

The LHWs are generated by cross-field ion motions produced by shocks. A fraction of preshock ions are reflected back upstream ahead of the shock with a velocity relative to the preshock plasma of $\sim 2v_s$, where v_s is the shock velocity. Ions reflected initially back along the shock velocity vector at a perpendicular shock travel a distance of $0.68v_s/\Omega_i$ before returning (Gedalin 1996). Here Ω_i is the ion gyrofrequency. The maximum distance ahead of the shock that reflected ions can reach is $d = 1.37v_s/\Omega_i$. This obtains for ions reflected from the shock at an angle of 30° to the shock front, so that $2v_s \sin 30^\circ = v_s$.

Consider a shock front at an angle θ to the local magnetic field direction. In order for the LHWs generated ahead of the shock by the reflected ion precursor to grow to large amplitudes (i.e., for the wave group velocity away from the shock to be equal to the shock velocity, so that the time available for wave growth is essentially unlimited on the timescale of these processes; Laming 2001b), we require

$$\frac{\partial\omega}{\partial k_\perp} = \frac{v_s}{\cos\theta} = \frac{\alpha\omega}{k_\perp}\ , \tag{A1}$$

where $\alpha = 1/(2\cos\beta\cos\theta)$ and β is the angle between $\partial\omega/\partial\boldsymbol{k}$ and the reflected ion bulk velocity vector $\boldsymbol{U}$. A minimum requirement for wave growth is $-1 < \alpha < -\frac{1}{2}$. Since it is ions *returning* to the shock that can generate the necessary waves, waves generated at the earliest possible period in the reflected ion orbit, i.e., the lowest value of $|\cos\beta|$, when $\alpha \sim -1$ (for $\cos\theta \sim 1$) will dominate the growth.

The maximum electric field that the LHW can develop before ion trapping and heating set in is given by Karney (1978) in mks units:

$$E = B\left(\frac{\Omega_i}{\omega}\right)^{1/3}\frac{\omega}{4k_\perp} \simeq B\left(\frac{\Omega_i}{\omega}\right)^{1/3}\frac{v_s}{4\cos\theta}\ . \tag{A2}$$

Taking the wave frequency $\omega = \Omega_{\mathrm{LH}} = (\Omega_i\Omega_e)^{1/2}$ and the component of the electric field directed along the magnetic field direction to be $E\omega_{pi}/\omega_{pe}$ gives $a \simeq \Omega_{\mathrm{LH}}(zm_e/m_i)^{1/6}v_s/4\cos\theta$ for electron acceleration along the magnetic field direction. The quantity Ω_{LH} is the geometric mean of the ion and electron gyrofrequencies and is known as the lower hybrid frequency.

We treat the case of a nonrelativistic shock that may accelerate electrons to relativistic energies. We work in the rest frame of the preshock medium. In this frame an electron is accelerated by the component of the electric field directed along the magnetic field until it outruns the reflected ion shock precursor a distance d from the shock front. Assuming acceleration begins with the electron at the shock front moving along $\boldsymbol{B}$ with initial velocity v_0, it will continue for a time t given by

$$\left[\frac{c^2}{a}\sqrt{1 + \frac{\left(at + v_0/\sqrt{1 - v_0^2/c^2}\right)^2}{c^2}} - \frac{c^2}{a\sqrt{1 - v_0^2/c^2}}\right]\sin\theta = d + v_s t\ , \tag{A3}$$

which gives a quadratic equation for t:

$$t^2\left(c^2\sin^2\theta - v_s^2\right) + t\left[\frac{2c^2}{a\sqrt{1 - v_0^2/c^2}}\left(v_0\sin^2\theta - v_s\sin\theta\right) - 2dv_s\right] - d^2 - \frac{2dc^2\sin\theta}{a\sqrt{1 - v_0^2/c^2}} = 0\ . \tag{A4}$$

We require $\sin\theta \geq v_s/v_0$ in order for the electron to stay ahead of the shock front, and the maximum acceleration time will be

realized for $\sin\theta = v_s/v_0$. In this case $\cos\theta \simeq 1$, the term linear in t in equation (A4) simplifies to $-2dv_s t$, and

$$t = \frac{d}{v_s\left(c^2/v_0^2 - 1\right)}\left[1 + \sqrt{1 + \left(\frac{c^2}{v_0^2} - 1\right)\left(1 + \frac{2c^2}{adv_0v_s\sqrt{1 - v_0^2/c^2}}\right)}\right]. \quad \text{(A5)}$$

For $v_0 \ll c$, $at = \left(2adv_0/v_s\right)^{1/2}$, and for $v_0 \sim c$, $at = 2ad/vs\left(c^2/v_0^2 - 1\right)$. Since $ad \propto v_s^2$, it is easy to see that the highest electron energies are most efficiently reached by fast shocks in hot plasma, i.e., for the highest plausible values of v_s and v_0 in Cas A. At $\sin\theta = v_s/v_0$, three to four shock interactions are required to accelerate electrons to the observed maximum energy of $\sim$95 keV, increasing to about 10 shock interactions if $\sin\theta = 1.2v_s/v_0$ for $v_s = 3000$ km s^{-1} and $v_0 = 3 \times 10^9$ cm s^{-1} (corresponding to an electron temperature of 4×10^7 K). Even faster shocks require fewer interactions. The maximum energy in the accelerated electron distribution will be determined by the number and obliquity of shock interactions experienced by these electrons during the evolution of Cas A and so for the time being remains uncertain. However, the maximum energy inferred from Figure 1 is certainly plausible in these terms. In principle, given enough shock interactions, relativistic electrons can be produced. If a means of transporting these electrons to the forward shock were available, this might have a bearing on providing an injection mechanism for further electron acceleration by a Fermi mechanism.

The normalization of the nonthermal bremsstrahlung spectrum is determined by the fraction of plasma electrons that are accelerated in this way, and this will be determined ultimately by a marginal stability criterion. The instability requires the electron gyroradius to be less than the wavelength divided by 2π, and once a sufficient number of electrons are accelerated to heat the ambient plasma to temperatures higher than this, the instability will shut down. The ambient plasma loses energy through radiation, adiabatic expansion, and possibly conduction. In Laming (2001b), the heating rate due to the observed accelerated electrons is estimated to be $4 \times 10^{-18} n_e n'_e$ ergs cm^{-3} s^{-1} for ambient and accelerated electron densities n_e and n'_e. The electron heating rate is $dT/dt = 0.019 n'_e$ K s^{-1}, and equating this to the cooling rate by adiabatic expansion of the Cas A remnant yields an accelerated electron fraction $n'_e/n_e \sim 0.02$. The inclusion of ionization and radiative power losses and relaxing the steady state assumption inherent in this estimate will allow higher accelerated electron fractions.

In Laming (2001b) an accelerated electron fraction of 4% was found to give a good match to the $\sim$50 ks of *BeppoSAX* MECS and PDS data on Cas A then available. The estimate herein using only the $\sim$500 ks PDS data is higher at around 10% (see Fig. 1), but a range of plasma temperatures exists in Cas A (e.g., Vink et al. 1996; Willingale et al. 2002b), and only the hottest plasma with a temperature of $\sim 4 \times 10^7$ K contributes to the PDS bandpass. Therefore, with respect to all the hot plasma, an accelerated electron fraction of $\sim$4% is consistent with the data and is preferred on theoretical grounds. Simulations of the evolution of the electron temperature following electron heating indicate that such an accelerated electron density heats plasma in the location of the contact discontinuity to temperatures in the range of $(4\text{–}5) \times 10^7$ K. These temperatures are basically constant over the past $\sim$30 yr over which X-ray observations have been made. In this respect, simulations of Cas A expanding into a $\rho \propto 1/r^2$ circumstellar medium appear to represent the physics much better than the simulations using a uniform-density circumstellar medium in Laming (2001b).

REFERENCES

Aharonian, F., et al. 2001, A&A, 370, 112
Ahmad, I., et al. 1998, Phys. Rev. Lett., 80, 2550
Allen, G. E., et al. 1997, ApJ, 487, L97
Anders, E., & Grevesse, N. 1989, Geochim. Cosmochim. Acta, 53, 197
Anderson, M. C., & Rudnick, L. 1996, ApJ, 456, 234
Arnaud, K. A. 1996, in ASP Conf. Ser. 101, Astronomical Data Analysis Software and Systems V, ed. G. Jacoby & J. Barnes (San Francisco: ASP), 17
Ashworth, W. B. 1980, J. Hist. Astron., 11, 1
Asvarov, A. I., Dogiel, V. A., Guseinov, O. H., & Kasumov, F. K. 1990, A&A, 229, 196
Atoyan, A., Tuffs, R. J., Aharonian, F. A., & Völk, H. J. 2000, A&A, 354, 915
Baars, J. W. M., Genzel, R., Pauliny-Toth, I. I. K., & Witzel, A. 1977, A&A, 61, 99
Balbus, S. A., & Hawley, J. F. 1992, ApJ, 400, 610
———. 1998, Rev. Mod. Phys., 70, 1
Begelman, M. C., & Chiueh, T. 1988, ApJ, 332, 872
Bell, A. R. 1978, MNRAS, 182, 147
Berezhko, E. G., Ksenofontov, L. T., & Völk, H. J. 2002, A&A, 395, 943
Biermann, P. L., & Cassinelli, J. P. 1993, A&A, 277, 691
Bingham, R., Kellett, B. J., Dawson, J. M., Shapiro, V. D., & Mendis, D. A. 2000, ApJS, 127, 233
Bleeker, J. A. M., Willingale, R., van der Heyden, K., Dennerl, K., Kaastra, J. S., Aschenbach, B., & Vink, J. 2001, A&A, 365, L225
Blumenthal, G. R., & Gould, R. J. 1970, Rev. Mod. Phys., 42, 237
Braun, R. 1987, A&A, 171, 233
Bykov, A. M., & Uvarov, Y. A. 1999, J. Exp. Theor. Phys., 88, 465
Cowsik, R., & Sarkar, S. 1980, MNRAS, 191, 855
Esposito, J. A., Hunter, D. A., Kanbach, G., & Skreekumar, P. 1996, ApJ, 461, 820
Favata, F., et al. 1997, A&A, 324, L49
Frontera, F., et al. 1997, A&AS, 122, 357
Gedalin, M. 1996, J. Geophys. Res., 101, 4871
Ginzburg, V. L., & Syrovatskii, S. I. 1965, ARA&A, 3, 297
Görres, J., et al. 1998, Phys. Rev. Lett., 80, 2554
Gotthelf, E. V., Koralesky, B., Rudnick, L., Jones, T. W., Hwang, U., & Petre, R. 2001, ApJ, 552, L39
Gringauz, K. I., et al. 1986, Nature, 321, 282
Haug, E. 1997, A&A, 326, 417
Huba, J. D. 1994, NRL Plasma Formulary (Washington, DC: Naval Res. Lab.)
Hwang, U., Holt, S., & Petre, R. 2000, ApJ, 537, L119
Iyudin, A. F., et al. 1994, A&A, 284, L1
Johnson, W. N., et al. 1993, ApJS, 86, 693
Kaastra, J. S., Mewe, R., & Nieuwenhuizen, H. 1996, Proc. 11th Colloq. on UV and X-ray Spectroscopy of Astrophysical and Laboratory Plasmas, ed. K. Yamashita & T. Watanabe (Tokyo: Universal Academy Press), 411
Karney, C. F. F. 1978, Phys. Fluids, 21, 1584
Klimov, S. S., et al. 1986, Nature, 321, 292
Koyama, K., Petre, R., Gotthelf, E. V., Hwang, U., Matsura, M., Ozaki, M., & Holt, S. S. 1995, Nature, 378, 255
Krasnosel'skikh, V. V., Kruchina, E. N., Thejappa, G., & Volokitin, A. S. 1985, A&A, 149, 323
Lagage, P. O., Claret, A., Ballet, J., Boulanger, F., Cesarsky, C. J., Cesarsky, D., Fransson, C., & Pollock, A. 1996, A&A, 315, L273
Laming, J. M. 2001a, ApJ, 546, 1149
———. 2001b, ApJ, 563, 828
Longair, M. S. 1994, High Energy Astrophysics, Vol. 2: Stars, the Galaxy, and the Interstellar Medium (2d ed.; Cambridge: Cambridge Univ. Press)
Lucek, S. G., & Bell, A. R. 2000, MNRAS, 314, 65
Norman, E. B., et al. 1998, Phys. Rev. C, 57, 2010
Nozawa, S., Itoh, N., & Kohyama, Y. 1998, ApJ, 507, 530
Quataert, E., Dorlan, W., & Hammet, G. 2002, ApJ, 577, 524
Reed, J. E., Hester, J. J., Fabian, A. C., & Winkler, P. F. 1995, ApJ, 440, 706
Reynolds, S. P. 1998, ApJ, 493, 375

Reynolds, S. P., & Keohane, J. W. 1999, ApJ, 525, 368
Schönfelder, V., et al. 2000, in AIP Conf. Proc. 510, 5th Compton Symp., ed. M. L. McConnell & J. M. Ryan (Melville: AIP), 54
Shapiro, V. D., Bingham, R., Dawson, J. M., Dobe, Z., Kellett, B. J., & Mendis, D. A. 1999, J. Geophys. Res., 104, 2537
Strong, A. W., Bloemen, H., Collmar, W., Diehl, R., Hermsen, W., Iyudin, A., Schönfelder, V., & The, L.-S. 2000, in AIP Conf. Proc. 510, 5th Compton Symp., ed. M. L. McConnell & J. M. Ryan (Melville: AIP), 60
Tanimori, T., et al. 1998, ApJ, 497, L25
The, L.-S., Leising, M. D., Kurfess, J. D., Johnson, W. N., Hartmann, D. H., Gehrels, N., Grove, J. E., & Purcell, W. R. 1996, A&AS, 120, 357
Thompson, A. C. 2001, X-Ray Data Booklet (Berkeley: Lawrence Berkeley Natl. Lab.)
Vaisberg, D. L., Galeev, A. A., Zastenker, G. N., Klimov, S. I., Nozdrachev, M. N., Sagdeev, R. Z., Sokolov, A. Y., & Shapiro, V. D. 1983, Soviet Phys.–JETP, 58, 716
Vink, J., Bloemen, H., Kaastra, J. S., & Bleeker, J. A. M. 1998, A&A, 339, 201
Vink, J., Kaastra, J. S., & Bleeker, J. A. M. 1996, A&A, 307, L41
Vink, J., & Laming, J. M. 2003, in Proc. XXII Moriond Astrophys. Meeting, The Gamma-Ray Universe, ed. A. Goldwurm, D. Neumann, & J. T. T. Van (Hanoi: Gioi), in press
Vink, J., Laming, J. M., Kaastra, J. S., Bleeker, J. A. M., Bloemen, H., & Oberlack, U. 2001, ApJ, 560, L79
Willingale, R., Bleeker, J. A. M., van der Heyden, K. J., & Kaastra, J. S. 2002a, A&A, submitted (astro-ph/0207273)
Willingale, R., Bleeker, J. A. M., van der Heyden, K. J., Kaastra, J. S., & Vink, J. 2002b, A&A, 381, 1039
Wright, M., Dickel, J., Koralesky, B., & Rudnick, L. 1999, ApJ, 518, 284